Abrogation of EMILIN1-β1 integrin interaction promotes experimental colitis and colon carcinogenesis

Alessandra Capuano[a], Eliana Pivetta[a], Giulio Sartori[a,1], Giulia Bosisio[a], Andrea Favero[a], Eleonora Cover[a], Eva Andreuzzi[a], Alfonso Colombatti[a], Renato Cannizzaro[b], Eugenio Scanziani[c,d], Lucia Minoli[c,d], Francesco Bucciotti[a], Ana Isabel Amor Lopez[e], Katya Gaspardo[f], Roberto Doliana[a], Maurizio Mongiat[a,2] and Paola Spessotto[a,2]

a - Unit of Molecular Oncology, *Centro di Riferimento Oncologico di Aviano (CRO), IRCCS, Aviano, Italy*
b - Unit of Oncological Gastroenterology, *Centro di Riferimento Oncologico di Aviano (CRO), IRCCS, Aviano, Italy*
c - Department of Veterinary Medicine, *University of Milan, Milan, Italy*
d - Mouse and Animal Pathology Lab (MAPLab), *Fondazione Filarete, Milan, Italy*
e - Microenvironment and Metastasis Group, *Molecular Oncology Program, Spanish National Cancer Research Centre (CNIO), Madrid, Spain*
f - Unit of Immunopathology and Cancer Biomarkers, *Centro di Riferimento Oncologico di Aviano (CRO), IRCCS, Aviano, Italy*

Correspondence to Roberto Doliana and Paola Spessotto: *at: Unit of Molecular Oncology, Centro di Riferimento Oncologico di Aviano (CRO), IRCCS, 33081 Aviano, Italy.* *rdoliana@cro.it*
https://doi.org/10.1016/j.matbio.2019.08.006

Abstract

Colon cancer is one of the first tumor types where a functional link between inflammation and tumor onset has been described; however, the microenvironmental cues affecting colon cancer progression are poorly understood. Here we demonstrate that the expression of the ECM molecule EMILIN-1 halts the development of AOM-DSS induced tumors. In fact, upon AOM-DSS treatment the *Emilin1*$^{-/-}$ (*E1*$^{-/-}$) mice were characterized by a higher tumor incidence, bigger adenomas and less survival. Similar results were obtained with the E933A EMILIN-1 (E1-E933A) transgenic mouse model, expressing a mutant EMILIN-1 unable to interact with α4/α9β1 integrins. Interestingly, upon chronic treatment with DSS, *E1*$^{-/-}$ and E1-E933A mice were characterized by the presence of increased inflammatory infiltrates, higher colitis scores and more severe mucosal injury respect to the wild type (*E1*$^{+/+}$) mice. Since alterations of the intestinal lymphatic network are a well-established feature of human inflammatory bowel disease and EMILIN-1 is a key structural element in the maintenance of the integrity of lymphatic vessels, we assessed the lymphatic vasculature in this context. The analyses revealed that both *E1*$^{-/-}$ and E1-E933A mice displayed a higher density of LYVE-1 positive vessels; however, their functionality was severely compromised after colitis induction. Taken together, these results suggest that the loss of EMILIN-1 expression may cause the reduction of the inflammatory resolution during colon cancer progression due to a decreased lymph flow and impaired inflammatory cell drainage.

Introduction

The ECM glycoprotein EMILIN-1 interacts with α4β1 [1], and the closely related α9β1 [2,3] integrins, via the globular homotrimeric C-terminus gC1q domain, promoting cell adhesion and migration [1,4]. In addition, EMILIN-1 provides an ECM cue for a correct homeostatic proliferation [2]; accordingly, targeted inactivation of the *Emilin1* gene induces dermal and epidermal hyperproliferation [2]. The oncosuppressive activity of EMILIN-1 has been preclinically demonstrated in the context of the

skin cancer, where we demonstrated that the absence of EMILIN-1 accelerates tumor development and increases the number and size of skin tumors [5].

Colon cancers are among the first where the critical contribution of chronic inflammation and the microenvironment towards tumor progression had been acknowledged. The colitis-associated cancer (CAC) is characterized by poor prognosis with a mortality rate of up to 15% [6]. This can at least in part be ascribed to the continuous cycles of tissue destruction and repair and with the persistent oxidative damage that can trigger mutagenesis and cancer initiation [7,8]. The development of aberrations that promote tumor initiation is strongly influenced by the contextual (i.e. inflammatory) microenvironment in which they arise as demonstrated by preclinical models of dextran sodium sulfate (DSS)-induced colitis [9]. Chronic inflammation contributes to tumorigenesis through direct and indirect mechanisms. It acts directly on cells increasing their proliferation and invasion and affecting the processes elicited during tissue repair; on the other side, it also induces changes in the microenvironment triggering the deposition of extracellular matrix (ECM) molecules and enhancing angiogenesis [10–13]. In addition, inflammation is associated with striking changes in the lymphatic vasculature [14] despite the molecular mechanisms involved in the regulation of this process are not completely understood. Proinflammatory cytokines, e.g., IL-1 and TNFα, are known to induce VEGF-C/D expression in infiltrating cells, thus supporting inflammatory lymphangiogenesis [14]. The formation of lymphatic vessels (LVs) in turn aids the resolution of inflammation allowing the drainage of tissue edema and the clearance of inflammatory cells [15]. It is currently accepted that alterations of LVs are a well-established feature of human and experimental inflammatory bowel disease [16] and can lead to a vast array of consequences, including persistence of the inflammatory process [17]. However, the tissue responses to the interplay between local chronic inflammation, ECM remodeling, and lymphangiogenesis in determining the fate of CAC are still poorly understood.

Another important direct role is played by EMILIN-1 in the growth and maintenance of LVs. Specifically, we have demonstrated that EMILIN-1 is part of the anchoring filaments, structural elements that connect lymphatic endothelial cells (LECs) with the ECM where it regulates the proper growth of lymphatic capillaries [18]. We also showed that its interaction with integrin α9 is required for the valve formation and maintenance of lymphatic collectors [3]. Finally, we found that EMILIN1 integrity is essential to guarantee the stability of LEC junctions [19]. Very recently, exploiting a transgenic mouse model carrying the E933A mutation in the gC1q domain of EMILIN-1 which abrogates the interaction with α4 and α9 integrins, we provided evidence for a novel "regulatory structural" role of EMILIN-1 in lymphangiogenesis [20,21].

Collectively, all these findings suggested that EMILIN-1 could play a relevant role in CAC. In the present study, we demonstrated that EMILIN-1, by virtue of its interaction with β1 integrins, is centrally located in the contest of CAC by controlling the process of proliferation, tumor development and by counteracting lymphatic dysfunction associated with chronic colonic inflammation.

Results

Emilin1$^{-/-}$ knock out (*E1*$^{-/-}$) and transgenic (E1-E933A) mice display higher susceptibility to the AOM-DSS-induced tumorigenesis

To verify if the expression of EMILIN-1 and the consequent interaction with its integrin receptor could halt tumor growth also in the context of colon cancer, we treated wild type (*E1*$^{+/+}$), knock out (*E1*$^{-/-}$) and transgenic (E1-E933A) mice with AOM-DSS (Fig. 1A), an established protocol of colon carcinogenesis that induces the onset of mutations through the mutagenic agent AOM and of inflammation following DSS treatment, thus recapitulating the traits of human colon cancer pathogenesis [22]. The development and growth of adenomas were next monitored and evaluated over time by endoscopy (Fig. 1B). At the end of the AOM/DSS treatment, colon samples were isolated, opportunely opened and washed to precisely evaluate all tumors (Fig. 1C). Tumor masses were assigned a score ranging from 1 to 5 with the highest score given to tumors occupying most of the colonic mucosa. Interestingly, these analyses indicated that the absence of functional EMILIN-1 was associated with a significant increase of the tumor lesions compared to the *E1*$^{+/+}$ animals; not only the number of tumors was higher but also the size, and the differences were even more striking in E1-E933A mice (Fig. 1D–E). In particular, only 50% of *E1*$^{+/+}$ treated mice developed proliferative lesions upon treatment; on the other hand, both *E1*$^{-/-}$ and E1-E933A mice were more prone to develop typical colonic tumors, particularly low and high-grade adenomas; in few cases, gastrointestinal intraepithelial neoplasias (GIN) were also detected (Fig. 1F–H). These results corroborated the anti-proliferative function of EMILIN-1 also in the context of the colonic mucosa, as we had previously demonstrated following induction of skin tumors [5]. Indeed, at the basal levels, the colon mucosae from *E1*$^{-/-}$ and E1-E933A mice displayed increased pro-proliferative signals such as increased phosphorylation of ERK1/2, and AKT as well as a higher number of Ki67-positive cells (Fig. 2). Moreover, results obtained in the transgenic E1-E933A

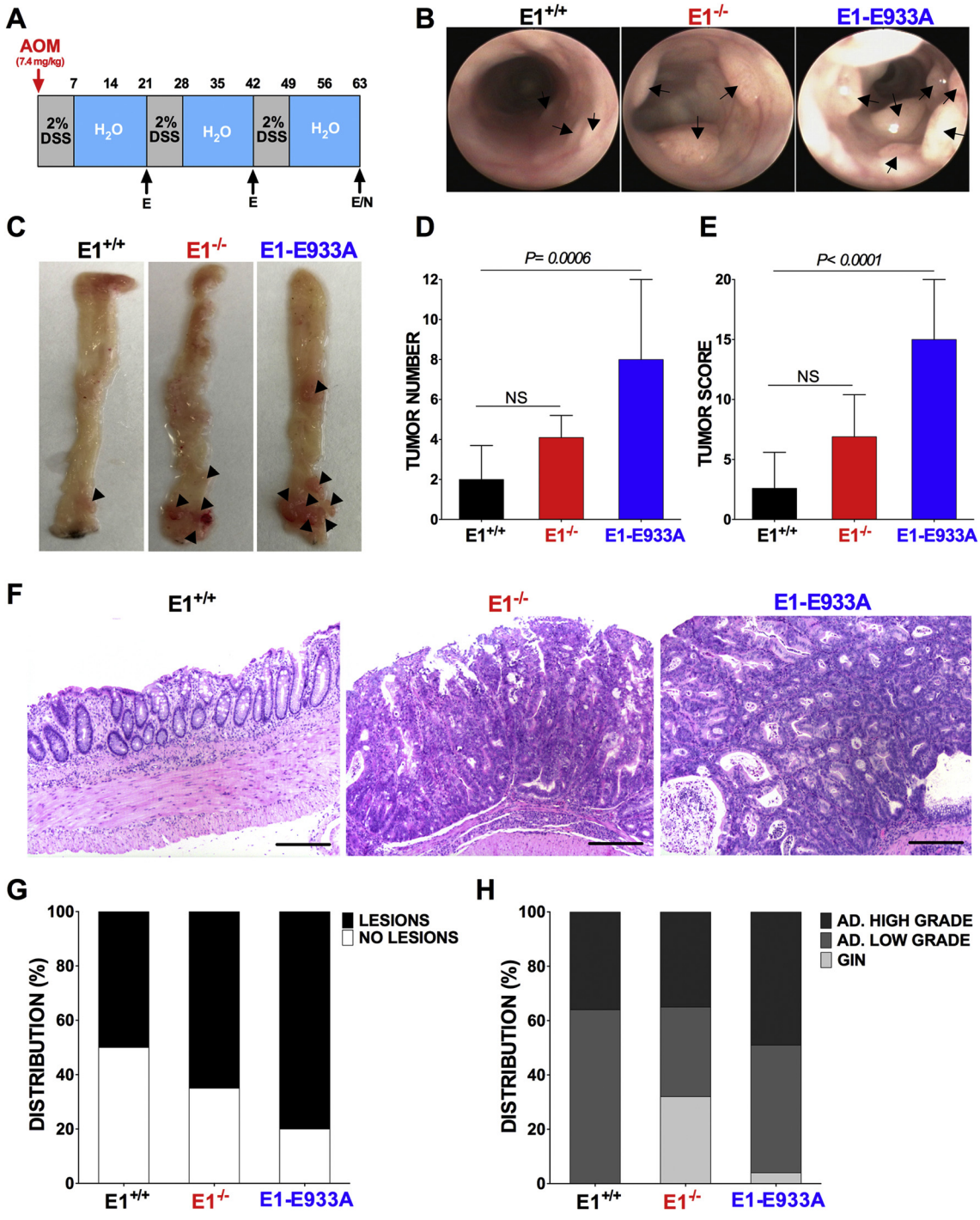

Fig. 1. Tumor incidence and severity are increased in E1$^{-/-}$ and E1-E933A transgenic mice. E1$^{+/+}$, E1$^{-/-}$ and E1-E933A C57BL/6J mice (n = 10 for each genotype) were given one dose of AOM intraperitoneally followed by one week-exposures of 2% DSS in the drinking water; at the end of the treatment (day 63), colon samples were fixed and paraffin embedded; 4 μm-thick sections were submitted to histopathological analysis in a blind fashion. (A) Schedule of treatments. (B) Representative endoscopic images of colon from the indicated groups of mice at day 42; arrows indicate visible tumors. (C) Representative pictures of gross anatomy examination of opened colons; arrowheads indicate main lesions. (D) Tumor number and (E) tumor score evaluated at necropsy (data shown as mean ± SD; statistical analysis: Mann Whitney *U* test). (F) Representative H&E-stained images of colon at the end of the experiment; scale bar: 100 μm. (G) Percentage of colon samples presenting (black) or not (white) proliferative lesions. (H) Histological classification of proliferative lesions and their distribution (%) among mice with different genotypes (GIN, gastrointestinal intraepithelial neoplasia; HG, high grade adenoma; LG, low grade adenoma).

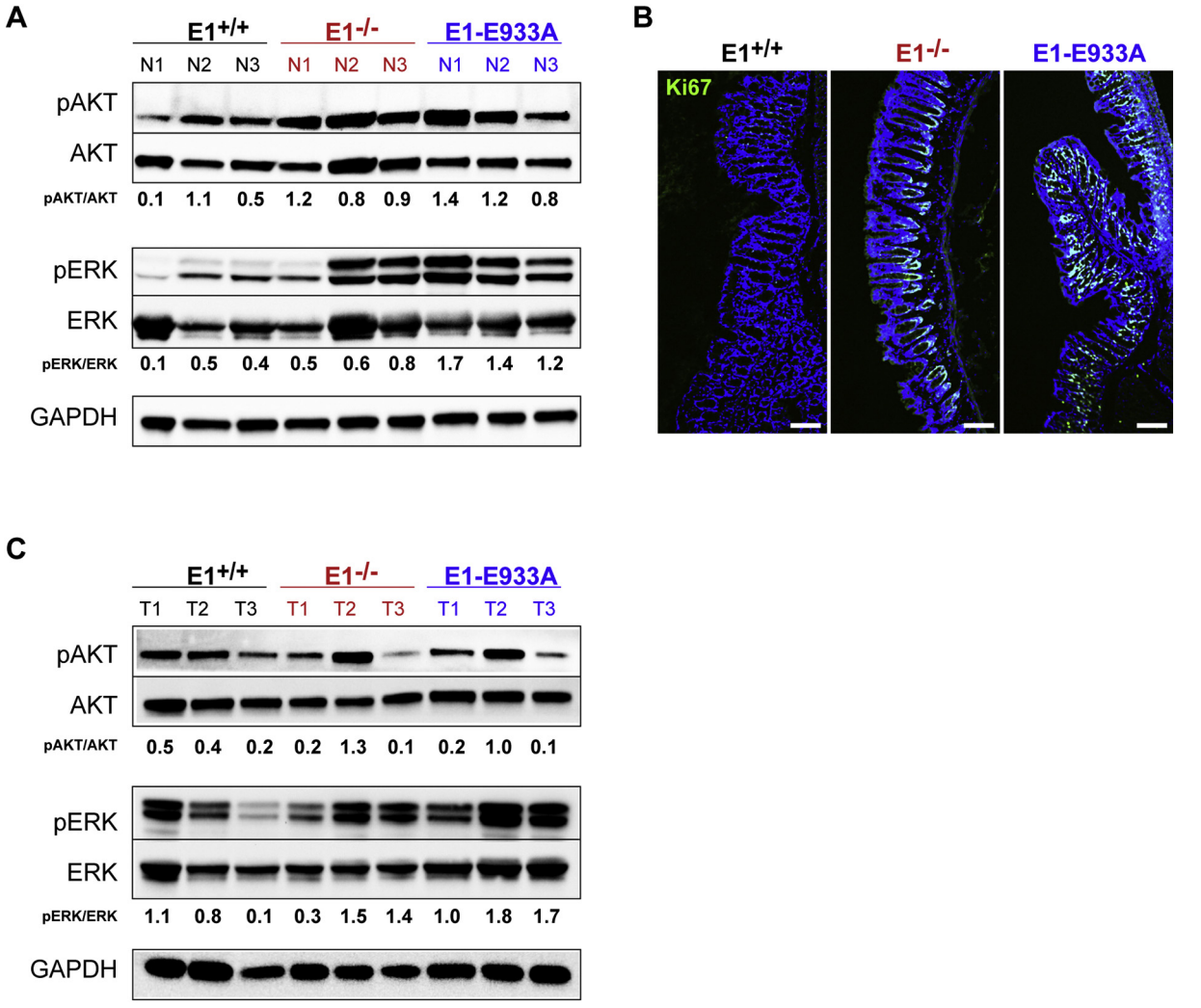

Fig. 2. E1$^{-/-}$ and E1-E933A colonic tissues display increased AKT and ERK activity. Western blotting analyses of normal (A) and tumor (C) colon extracts from 3 mice for each genotype and the corresponding pAKT/AKT and pERK/ERK quantification by QuantityOne software (N, normal; T, tumor). GAPDH was used as loading control. (B) Representative cryostat section images of untreated colon from E1$^{+/+}$, E1$^{-/-}$ and E1-E933A mice stained for the proliferation marker Ki67 (green). Nuclei are pseudocolored in blue. Scale bar, 100 μm.

mouse model suggest that this EMILIN-1 property was strictly related to the interaction between the gC1q domain with its integrin receptor.

According to the Disease Activity Index (DAI), which takes into account the extent of weight loss, the stool consistency and the presence of blood in stools (see Supplemental Table S1), we could conclude that, under treatment, the *E1*$^{-/-}$ and E1-E933A mice were characterized by the presence of more diffuse inflammation in the colonic mucosa respect to *E1*$^{+/+}$ counterpart (Fig. 3A). Similar results were obtained applying the murine endoscopic score of colitis severity (MEICS) which takes into account the thickening of the colon wall, changes in the vascular pattern, presence of fibrin, mucosal granularity and stool consistency (Fig. 3B and Supplemental Table S2). At the end of the experiment mice were sacrificed and the colons were isolated. Consistently, colons from *E1*$^{-/-}$ and E1-E933A treated mice were significantly shorter compared to those from the wild type counterpart, a clear indication of bowel inflammation [23] (Fig. 3C). In addition to the typical signs of diffuse inflammation in the colonic mucosa already evident in H&E stained colon sections (Fig. 1F), epithelial crypts of AOM/DSS-treated *E1*$^{-/-}$ and E1-E933A mice were distorted and irregularly distributed within the lamina propria (LP), which was abundantly infiltrated by inflammatory cells (Fig. 3D). The higher accumulation of inflammatory cells in the LP positively correlated to the general increase of white blood cells

(WBCs) detected in the peripheral blood samples (Figs. 3E–F and S1), despite the difference was not statistically significant. However, no predominant WBC population was observed (Figs. 3G and S1).

E1$^{-/-}$ and E1-E933A mice are more susceptible to DSS-induced experimental colitis

To avoid strain specific effects and different sensibility to DSS, we subjected both C57BL/6J and FVB mice (*E1*$^{+/+}$, *E1*$^{-/-}$ and E1-E933A) to a DSS-induced protocol of colitis and assessed if EMILIN-1 could influence the inflammatory response (Figs. 4A and S2A). Under normal conditions, colon length, colonic mucosa morphology and blood cell composition were very similar in all genotypes (Fig. S1). On the contrary, in both mouse strains, endoscopic examination showed a more severe inflammatory status in DSS-treated *E1*$^{-/-}$ and E1-E933A mice (Figs. 4B and S2B). *E1*$^{-/-}$ and E1-E933A mice suffered from a higher weight loss and displayed more serious rectal bleeding as envisioned from the DAI index (Figs. 4C and S2C). MEICS analyses indicated that *E1*$^{-/-}$ and E1-E933A mice displayed thicker mucosa characterized by a typical inflammatory granular pattern, copious fibrin accumulation, bleeding and vascular changes (Figs. 4D and S2D). On the contrary, *E1*$^{+/+}$ littermates exhibited moderate granularity, modest fibrin accumulation, and regular vascular architecture. Also the evaluation of colon length confirmed a greater inflammatory response in *E1*$^{-/-}$ and E1-E933A animals since the colons were thicker and shorter compared to the *E1*$^{+/+}$ counterpart (Figs. 4E and S2E). Despite the presence of slight differences between strains, no significant alterations of peripheral blood cell composition were observed, as observed upon AOM-DSS treatment (Figs. 4F–H and S2F–H).

Epithelial damage and the extent of the LP infiltrate were chosen as parameters for the histopathological evaluation of inflamed colonic samples. *E1*$^{-/-}$ and E1-E933A treated mice were more responsive to the colitis induction, with a worse histopathological pattern respect to *E1*$^{+/+}$ mice. In both C57BL/6J (Fig. 5A–B) and FVB (Fig. S3A–B) strains, *E1*$^{-/-}$ and especially E1-E933A mice displayed extensive epithelial damage, leading in some cases especially in the distal colon mucosa to squamous metaplasia, typical of ulcerative colitis, although its characteristic endoscopic appearance has been rarely described [24]. *E1*$^{-/-}$ and E1-E933A crypts were not well-defined and appeared irregular. On the other hand, *E1*$^{+/+}$ mice generally displayed a normal mucosa architecture and the majority of the crypts were not affected by the treatment (Figs. 5A–B and S3A–B). In addition, *E1*$^{-/-}$ and particularly E1-E933A treated mice were characterized by an increased recruitment of inflammatory cells compared to the *E1*$^{+/+}$ counterparts (Figs. 5A–C and S3A–C).

E1$^{-/-}$ and E1-E933A mice display an increased recruitment of inflammatory cells upon DSS treatment

We next analyzed in more detail the type of inflammatory cells recruited in the colon of the different mouse models upon DSS treatment. We found that only FVB *E1*$^{-/-}$ and E1-E933A but not C57Bl/6J *E1*$^{-/-}$ and E1-E933A treated mice showed an evident increased number of CD3^{+} and CD45/B220^{+} cells compared to the *E1*$^{+/+}$ mice (Figs. 6 and S4). More leukocytes were detected in *E1*$^{-/-}$ and E1-E933A treated mice (Figs. 6 and S4); indeed, Ly6G staining revealed a slight increase in neutrophil population in *E1*$^{-/-}$ and E1-E933A treated mice as well as a larger macrophage infiltrate as shown by Iba1 staining (Figs. 6 and S4). In any case, the differences were not statistically significant if compared to *E1*$^{+/+}$ animals.

Overall, *E1*$^{-/-}$ and E1-E933A treated mice were characterized by an extensive inflammation in comparison with the *E1*$^{+/+}$ counterparts; however, no predominant cell population apparently emerged as a characteristic driver of the inflammatory process.

The colons from *E1*$^{-/-}$ and E1-E933A mice are characterized by impaired lymphatic function

Recently, we demonstrated that in normal colon specimens LVs from both *E1*$^{-/-}$ and E1-E933A mice were irregular with narrowed and ring-shaped valves compared to *E1*$^{+/+}$ mice. Moreover, in all *E1*$^{-/-}$ and E1-E933A colonic samples analyzed, we also detected dysmorphic structures and wide lacunae (with lymph leakage) that were not detectable in colonic LVs of *E1*$^{+/+}$ mice [20].

As reported by many authors, the expansion of lymphatic network induced by the treatment with both DSS and AOM/DSS is required for a proper resolution of the inflammatory process [16,25,26]. Interestingly, the analyses of the LV network in inflamed areas of the colon revealed that, besides the already documented alterations in EMILIN-1 mutant mice, the size of LVs in both *E1*$^{-/-}$ and E1-E933A mice was increased compared to E1$^{+/+}$ animals in which some of the collectors displayed normal valves (Fig. 7A). Immunostaining of FFPE colon samples showed that the surface covered by Lyve-1 positive structures was higher in *E1*$^{-/-}$ and E1-E933A than in *E1*$^{+/+}$ mice (Fig. 7B). The increase of the Lyve-1 positive colonic areas was statistically significant in untreated and DSS-treated E1-E933A respect to E1$^{+/+}$ mice and confirmed that the induced inflammation caused lymphatic alterations that in mutant mice could also be documented by a larger LV diameter (Fig. 7B, arrows).

Indeed, further analyses suggested an impairment of LVs function, since lymphatic drainage was

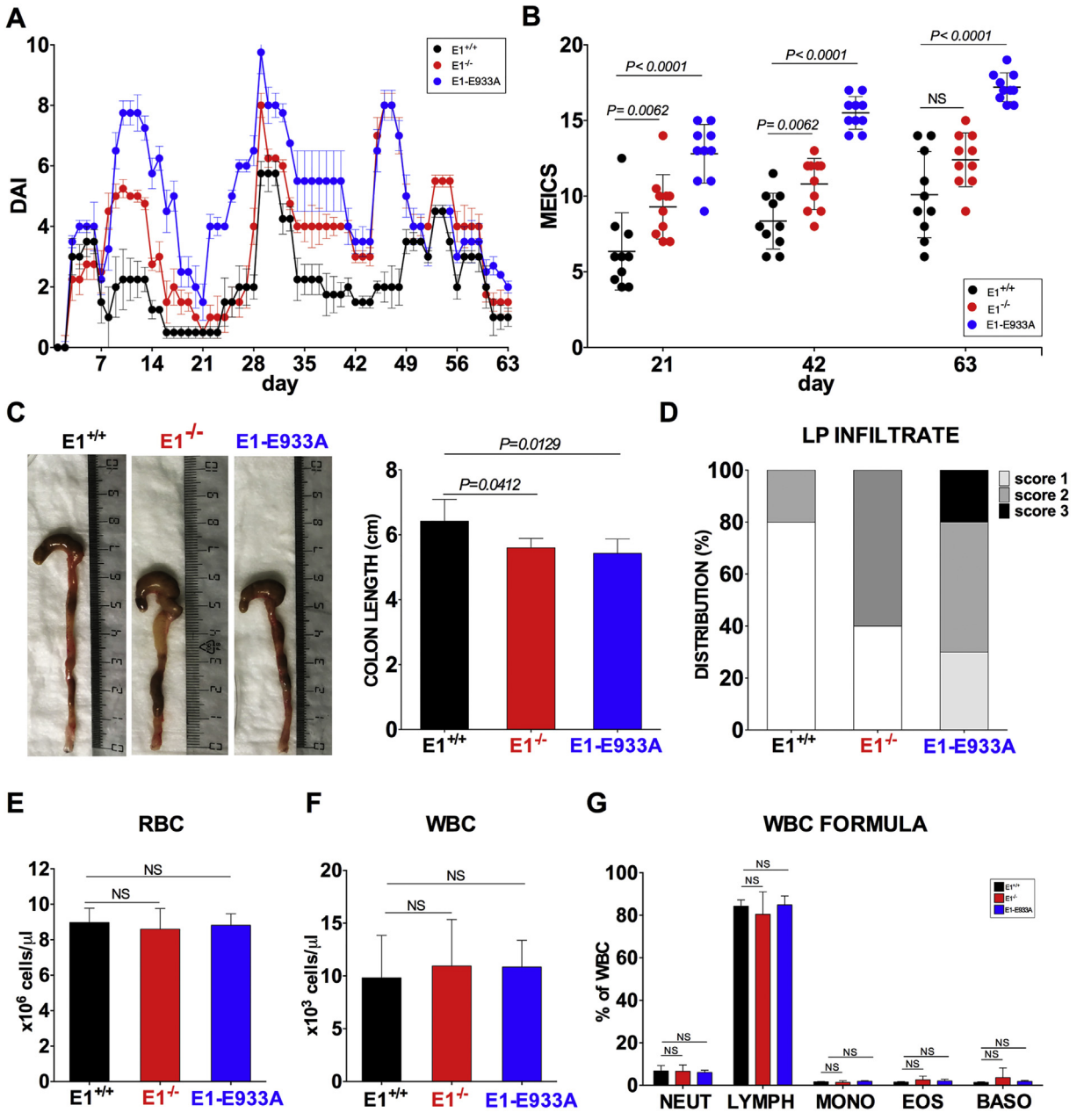

Fig. 3. E1$^{-/-}$ and E1-E933A transgenic mice are more prone to develop inflammation in a two-step AOM-DSS colon carcinogenesis model. AOM/DSS-treated C57BL/6J mice were analyzed for several colitis scores and inflammatory parameters. (A) Disease Activity Index (DAI). (B) Murine Endoscopic Index of Colitis Severity (MEICS). (C) Representative images of recovered closed colons from the indicated groups of mice (left) and colon length measured at necropsy (right). (D) Histopathological evaluation of the inflammatory infiltrate in the lamina propria (LP) of colons from the indicated groups of mice (*score 1*: absent/rare/few inflammatory cells; *score 2*: moderate number of inflammatory cells; *score 3*: numerous inflammatory cells); data are shown as score distribution (%) in the different genotypes. (E) Red blood cells, (F) white blood cells counts and (G) white blood cells formula from blood samples collected at the end of the experiment. NEU, neutrophils; LYMPH, lymphocytes; MONO, monocytes; EOS, eosinophils; BASO, basophils. Data are shown as mean ± SD; Mann Whitney U test was used for statistical analysis.

prejudiced in *E1*$^{-/-}$ and E1-E933A mice, as assessed through the oral gavage administration of fluorescently labeled Bodipy-FL-C_{16}, a 16-carbon chain fatty acid (Fig. 8). The DSS and AOM-DSS treatments exacerbated the altered lymphatic functionality in *E1*$^{-/-}$ and E1-E933A mice where mesenteric lymph nodes and LVs did not contain Bodipy-FL-C_{16} tracer after 2 h from the

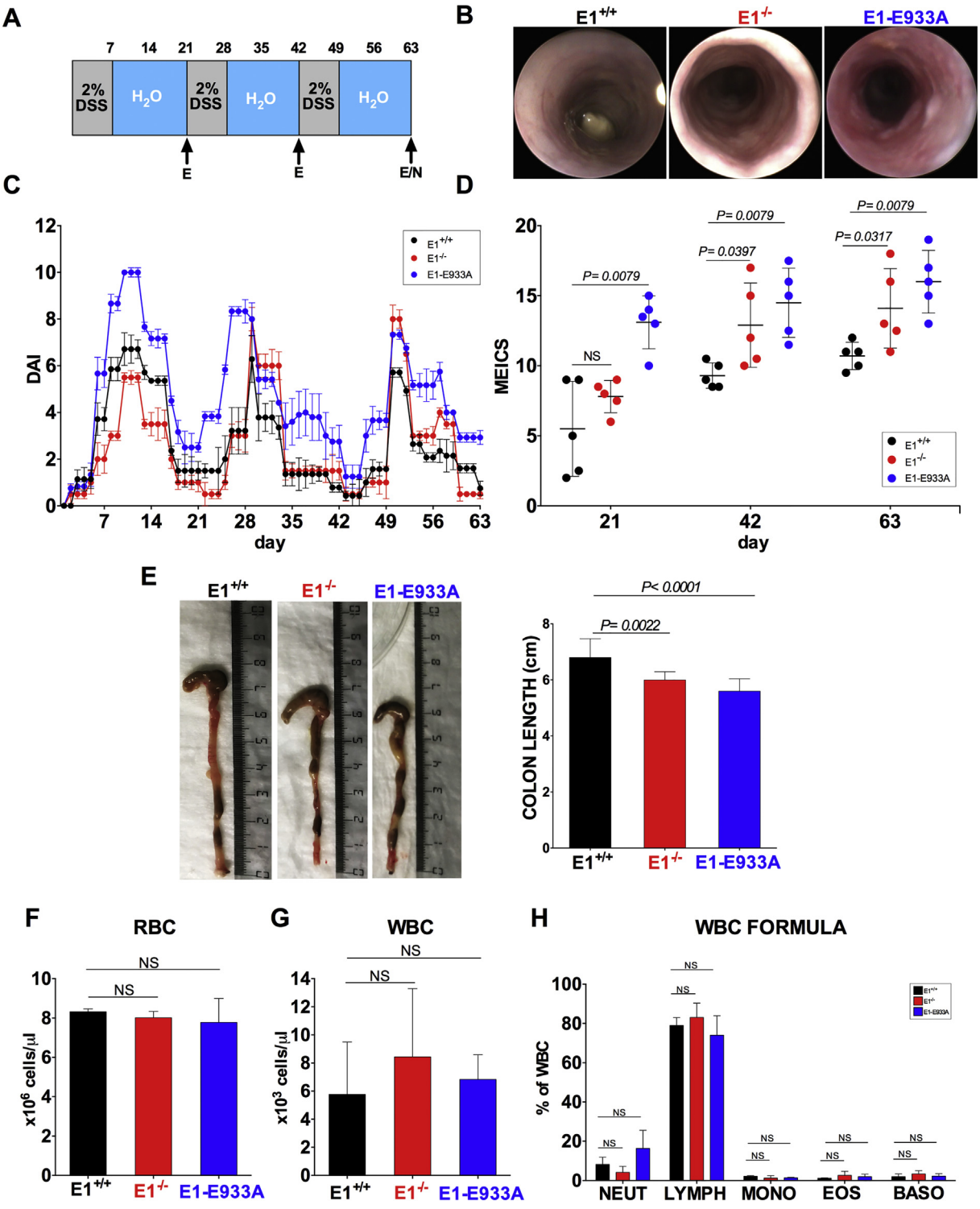

Fig. 4. The severity of DSS-induced chronic colitis is enhanced in E1$^{-/-}$ and E1-E933A transgenic mice. Chronic colitis was established in E1$^{+/+}$, E1$^{-/-}$ and E1-E933A C57BL/6J mice (n = 5 for each genotype) with three cycles of 2% DSS-exposure in the drinking water. (A) Schedule of treatments. (B) Representative endoscopic images of colons from the indicated groups of mice at day 42. (C) Disease Activity Index (DAI). (D) Murine Endoscopic Index of Colitis Severity (MEICS). (E) Representative images of closed colon recovered from the indicated groups of mice (left) and colon length measured at necropsy (right). (F) Red blood cells, (G) white blood cells counts and (H) white blood cells formula from blood samples collected at the end of the experiment. NEU, neutrophils; LYMPH, lymphocytes; MONO, monocytes; EOS, eosinophils; BASO, basophils. Data are shown as mean ± SD; Mann Whitney U test was used for statistical analysis.

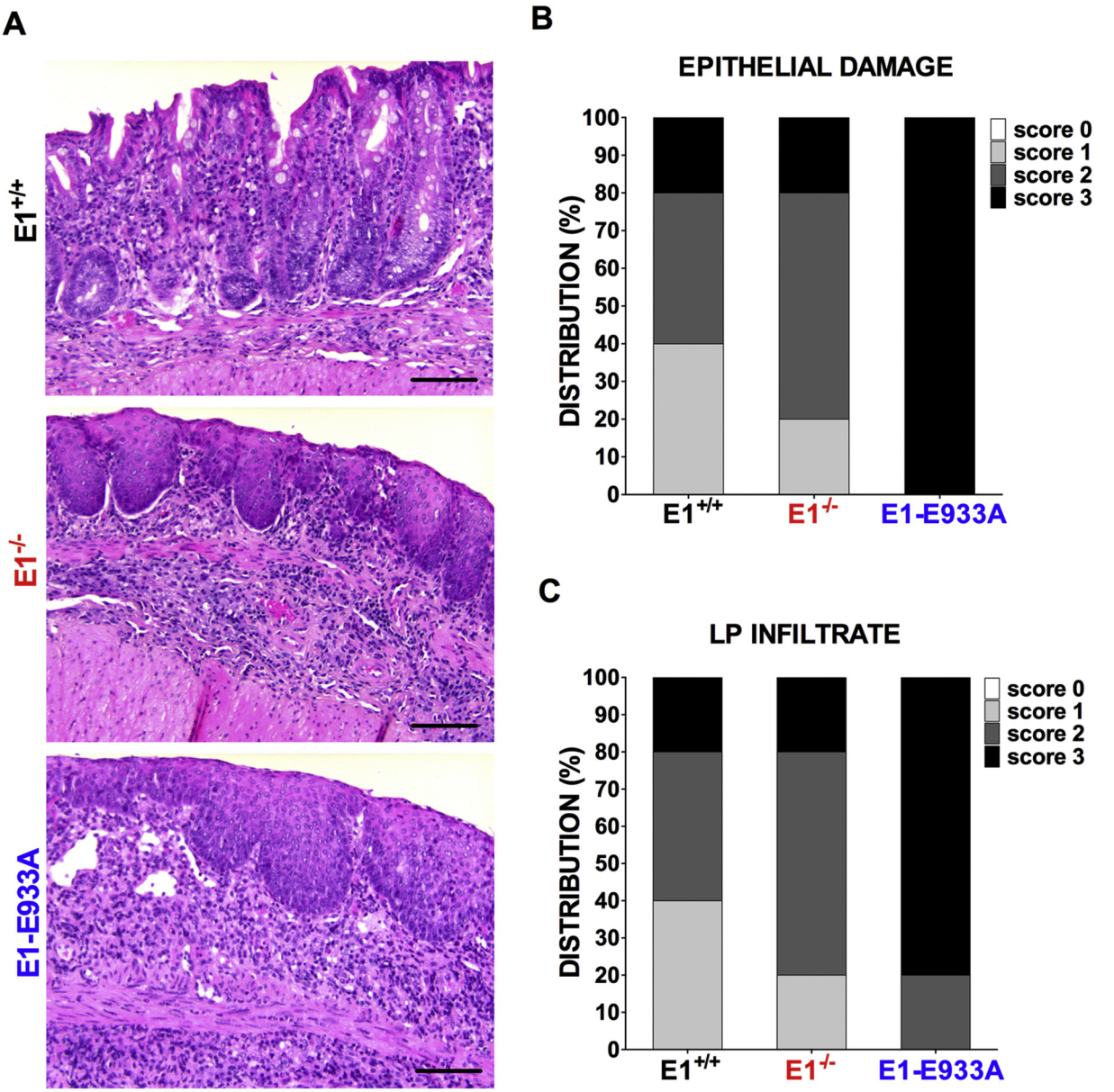

Fig. 5. $E1^{-/-}$ and E1-E933A transgenic mice develop more severe mucosal injury and present more abundant inflammatory infiltrates in DSS-induced chronic colitis. Colon samples from DSS-induced chronic colitis experiment were fixed and paraffin embedded; 5 μm-thick sections were submitted to histopathological analysis in a blind fashion. (A) Representative H&E-stained images of colons at the end of the experiment; scale bar: 100 μm. (B) Epithelial damage scoring (*score 0*: absent; *score 1*: rare; *score 2*: moderate; *score 3*: severe) and (C) inflammatory infiltrate evaluation (*score 1*: absent/rare/few inflammatory cells; *score 2*: moderate number of inflammatory cells; *score 3*: numerous inflammatory cells) in colons from the indicated groups of mice (data are shown as score distribution).

administration, whereas the lymphatic structures of treated *E1*$^{+/+}$ littermates were stained despite weakly by the Bodipy-FL-C_{16} tracer (Fig. 8).

The role of EMILIN-1 in promoting the formation of a proper and functional lymphatic vasculature was tested through the assessment of the activation of AKT and ERK, the major regulators of lymphangiogenesis [27,28]. Through its regulatory domain gC1q, EMILIN-1 was able to efficiently trigger AKT and ERK phosphorylation in LECs, similarly to what observed upon treatment with VEGF-C, a well-known lymphatic growth factor (Fig. 9A–C). The kinetics suggested that gC1q and VEGF-C signaled through different receptors that may cross-talk. As reported in literature, VEGF-C induced the highest VEGFR3 activation already at 10–15 min following

the treatment [29,30]. Interestingly, only the wild type gC1q domain but not the mutant E933A-gC1q was able to induce AKT and ERK activation to the same extent observed challenging LECs with VEGF-C; however, the activation was persistent and could be detected also after 30 min following the treatment (Fig. 9C). To verify if the engagement of EMILIN-1 could induce a cross-activation of VEGFR3 via the engagement of integrin $\alpha_9\beta_1$ expressed on LECs [3], the cells were challenged with gC1q and VEGFR3 was immunoprecipitated for western blotting analyses. These experiments revealed that gC1q was unable to phosphorylate VEGFR3 (Fig. 9D), suggesting that the integrin engagement could signal independently from the activation of VEGFR3.

Discussion

Several lines of evidence suggest that the constituents of the local ECM microenvironment and their multiple interactions may contribute to the pathogenesis of the inflammatory diseases. The accumulation of hyaluronic acid at sites of chronic inflammation creates a permissive tissue microenvironment for the development of autoimmune diseases [31]. In addition, fragments of collagen and elastin derived from the degradation activity of MMPs or other enzymes released by inflammatory cells play pathogenic roles in several common chronic inflammatory lung diseases and inflammatory bowel disease [32,33]. Post-translation modifications of ECM components, such as glycation, citrullination and carbamylation, can also play a major role in the regulation of the inflammatory disease [34]. A further layer of complexity in the modulation of the ECM molecular network in this context was recently ascribed to the action of the extracellular vesicles in the formation of niches suitable for tissue regeneration and inflammation [35].

Here, for the first time we demonstrated that the EMILIN-1/β_1 integrin interaction exerts a oncosuppressive role in the colon microenvironment, as it was previously well established in the context of the skin cancer [5]. Also in the colonic context, the mechanism involves the activation of AKT and ERK, and, following the induction of colon carcinogenesis, associates with a higher number of tumors (especially high-grade adenoma and GIN) of substantial larger size in both *E1* $^{-/-}$ and E1-E933A mice. These results reinforced the notion that EMILIN-1 is one among the very few ECM proteins, such as fibulin-2 [36], EMILIN-2 [37] and decorin [38], exerting a direct tumor suppressor function. Other components can play an anti-tumor activity through an indirect mechanism [39,40]; however, a large amount of ECM proteins promotes tumor growth and progression [41–46]. A similar outcome was obtained when we employed the E1-E933A transgenic mice characterized by the ectopic expression of an EMILIN-1 mutant in the gC1q domain, incapable of engaging the $\alpha_4/\alpha_9\beta_1$ integrin. These results suggested that the promotion of tumor growth depends on the lack of interaction with the integrin receptor, rather than an altered TGF-β signaling, since its maturation is regulated only by the EMI domain of EMILIN-1 [47]. The altered tumor growth, inflammatory response and lymphatic alterations were more evident when using E1-E933A mice as opposed to *E1* $^{-/-}$ mice. This could likely be due to the absence of the EMILIN-1 EMI domain in *E1* $^{-/-}$ mice, and the consequent increase of the TGF-β levels that can exert contrasting effects on cell proliferation as well as in the lymphangiogenic process [21,48,49]. Thus, the use of the E1-E933A mouse was useful and informative to discern the effects linked to the regulation of TGF-β by the EMI domain from those dependent on the EMILIN-1/integrin interaction.

A second finding of the AOM/DSS colon carcinogenesis approach was the demonstration that *E1* $^{-/-}$ and E1-E933A treated mice of two different strains (C57BL/6J and FVB) displayed more severe inflammation in the colonic mucosa respect to *E1* $^{+/+}$ mice. During the pathogenesis of inflammatory bowel disease, which is linked to CAC development, both the LP and the epithelial layer are infiltrated by different types of immune cells, which create an inflammatory microenvironment [50]. Our investigation indicates that EMILIN-1 deeply affects the inflammatory response since both *E1* $^{-/-}$ and E1-E933A mice displayed an increased infiltration of T and B cells, granulocytes and a slight but not statistically significant increase of macrophages in the inflamed colons. We also found that the levels of IL-1α, IL-1β and IL-6, which play a pro-inflammatory role during chronic inflammation, were slightly increased (data not shown). Nevertheless, we were not able to discriminate a specific inflammatory cell population that could predominantly drive a consistent development of tumors in the two-step colon carcinogenesis model. The presence of a non-resolving chronic inflammatory niche is typical of the gastrointestinal tumor microenvironment, as well as in other tumors [51]; what we observed in this study is that the absence of (functional) EMILIN-1 exacerbated the inflammatory status which was persistent and more aggressive.

Induction of intestinal inflammation is well known to require the presence of functional LVs and effective lymphatic drainage for its resolution. Indeed, the expansion of lymphatic vasculature is necessary to obtain fluid clearance and immune cell trafficking [26]. Our findings provide evidence that the lack of EMILIN-1 induces the formation of aberrant lymphangiogenesis with the generation of unfunctional LVs suggesting that this could cause the exacerbation of the disease. We in fact have previously shown that EMILIN-1 is crucial for the

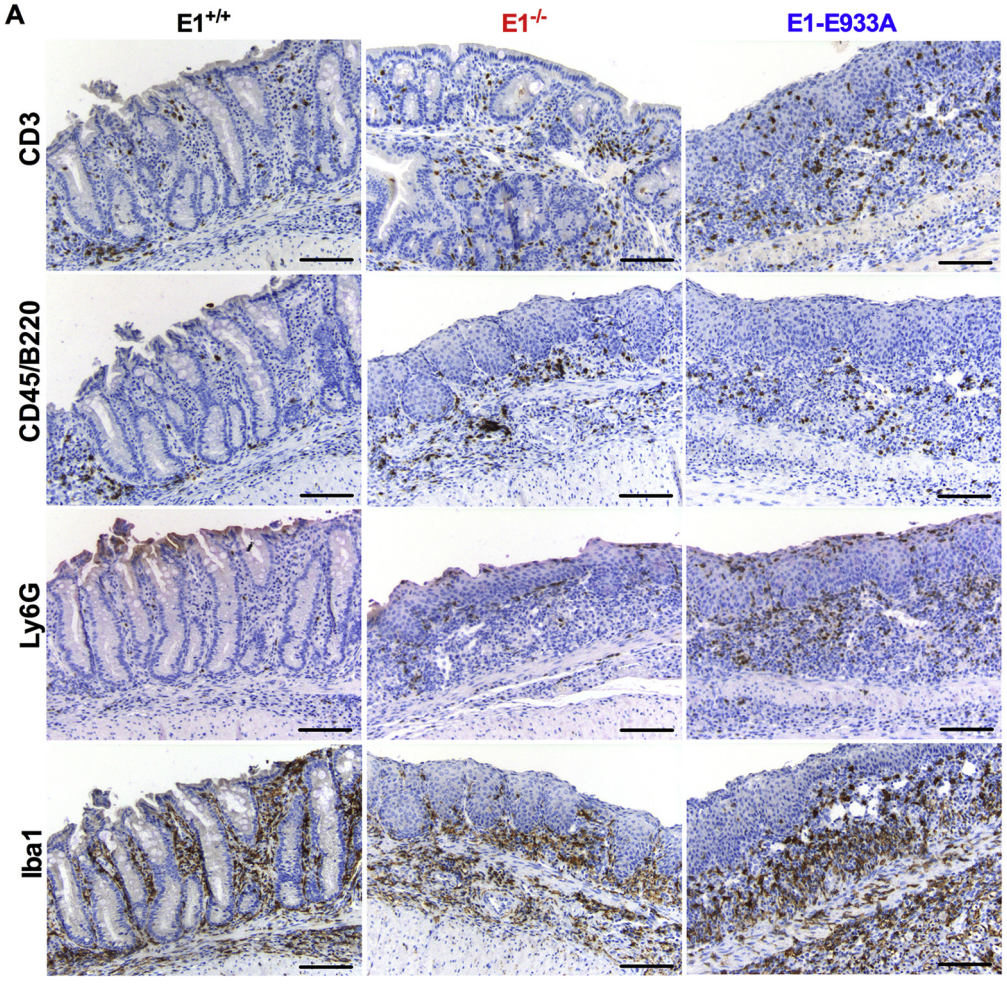
A
E1+/+
E1-/-
E1-E933A
CD3
CD45/B220
Ly6G
Iba1

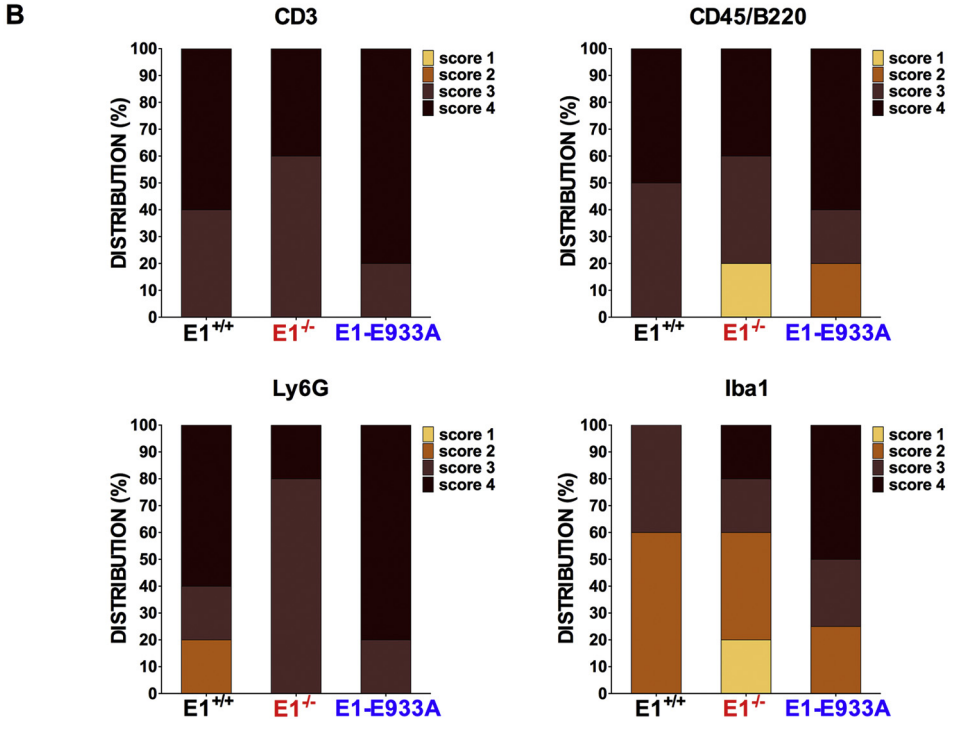
B
CD3
CD45/B220
Ly6G
Iba1
DISTRIBUTION (%)
score 1
score 2
score 3
score 4
E1+/+
E1-/-
E1-E933A

maintenance of a correct lymphatic vasculature [3,18,19,21]; in our recent study we demonstrated that EMILIN-1 promotes the formation of functional LVs through the gC1q domain [21] and in the present work we demonstrated that gC1q interacting with $\alpha_9\beta_1$ integrin was able to induce the activation of lymphangiogenesis pathway in LECs. Differently than what was already demonstrated $\alpha_5\beta_1$ integrin [52,53], a cross-talk between VEGFR3 and $\alpha_9\beta_1$ integrin expressed on LECs [3] very likely does not occur as shown by the absence of VEGFR3Tyr phoshorylation following stimulation by gC1q. The co-presence of both VEGF-C and gC1q induced a sustained and stronger activation, suggesting that a well-orchestrated lymphangiogenic response requires coordination between the integrin receptor and VEGFR3. This possibility is evinced by the fact that the treatment with exogenous VEGF-C is not sufficient for the formation of a correct new lymphatic vasculature [54]. The data provided in this study further highlight the regulatory role of ECM in this context and that the expression of EMILIN-1 is required in order to allow a proper formation of the lymphatic vasculature and, hence, a proper resolution of the inflammatory response. In fact, in the absence of treatment *E1*$^{-/-}$ and E1-E933A mice displayed altered lymphatic phenotype in the colon; however no significant differences in resident immune cell number and distribution were detected. Following DSS or AOM-DSS treatment all the mice models taken into account were characterized by the presence of an expanded lymphatic vasculature, but only in wild type animals the LVs were functional, as assessed by mesenteric lymphangiography. These results suggest the strong inflammatory stimulus induced by DSS led to the formation of new competent and functional vasculature only in *E1*$^{+/+}$ mice, thanks to the expression of a functional gC1q able to engage the integrin; in turn this allowed a proper drainage of the inflammatory cells and the restoring of the pre-inflammatory state. On the contrary, the impaired clearance of inflammatory cells in DSS-treated *E1*$^{-/-}$ and E1-E933A mice led to the onset of a severe inflammatory microenvironment. Thus, it is reasonable to assume that the harsh inflammatory condition observed in *E1*$^{-/-}$ and E1-E933A mice was the consequence of structural and functional lymphatic deregulation associated with a lack of EMILIN-1 and, in particular, of its functional gC1q domain.

These findings are conceptually innovative since to our knowledge, it is the first time that the lack of a specific domain in the tumor microenvironment leads to an exacerbated inflammatory response and tumor progression impinging on the efficiency of the LVs. Thus since the *E1*$^{-/-}$ and E1-E933A mice are the only models showing that the lack of an ECM molecule associates with the formation of an altered lymphatic phenotype, they represent an ideal and precious tool to shed light on the possible mechanisms regulating the resolution of the inflammatory response in the tumor microenvironment. We have previously demonstrated that neutrophils-secreted elastase (NE) is responsible for the degradation of EMILIN-1 [19,55] and this could likely be a possible mechanism of EMILIN-1 loss. Indeed, colorectal cancer is characterized by the recruitment of massive inflammatory infiltrates, including macrophages and neutrophils that colonized the LP and submucosa [56–58]. The increased presence of these cells, and the consequent increase of the NE levels during colon cancer progression may thus cause a significant drop of the gC1q level in the microenvironment with a consequent loss of an important ligand for integrin $\alpha_4/\alpha_9\beta_1$. We have in fact demonstrated that the activity of NE is able to fully abrogate the gC1q/integrin interaction inducing a cleavage adjacent to the E933 binding site [55].

In conclusion, this study suggests that the degradation and consequent loss of EMILIN-1/gC1q in the tumor microenvironment may favor colon cancer initiation and progression in different ways: (I) abolishment of the EMILIN-1/gC1q oncosuppressive properties; (II) formation of dysfunctional LV; (III) exacerbation of the inflammatory response due to LV-born impairment of the inflammatory cell drainage. We envision that the blockage of gC1q degradation may represent a promising ECM-based therapeutic approach to rescue the control of proliferation, induce LV normalization and facilitate the resolution of the inflammatory response in colon cancer.

Materials and methods

Reagents

The recombinant wt and E933A-gC1q mutant were produced and purified as previously describe [1,60]. The pQE30 vector, Wizard SV columns for

Fig. 6. Inflammatory cell populations in DSS-induced chronic colitis samples. Mucosal tissues from DSS-induced chronic colitis experiment (in C57BL/6J strain) were immunostained for CD3 (T cell marker), CD45/B220 (B cell marker), Ly6G (neutrophil marker) and Iba1 (macrophage marker). (A) Panel of representative images for each cell population analyzed (scale bar: 100 μm). (B) Summary of immunohistochemical findings in the indicated groups of mice. Data are shown as score distribution for each treatment group; score were applied counting the number of positive cells in 3400× microscopic fields according the following criteria: *score 0* = 0 cells; *score 1* = 1–15 cells; *score 2* = 16–30 cells; *score 3* = 31–60 cells; *score 4* = >60 cells.

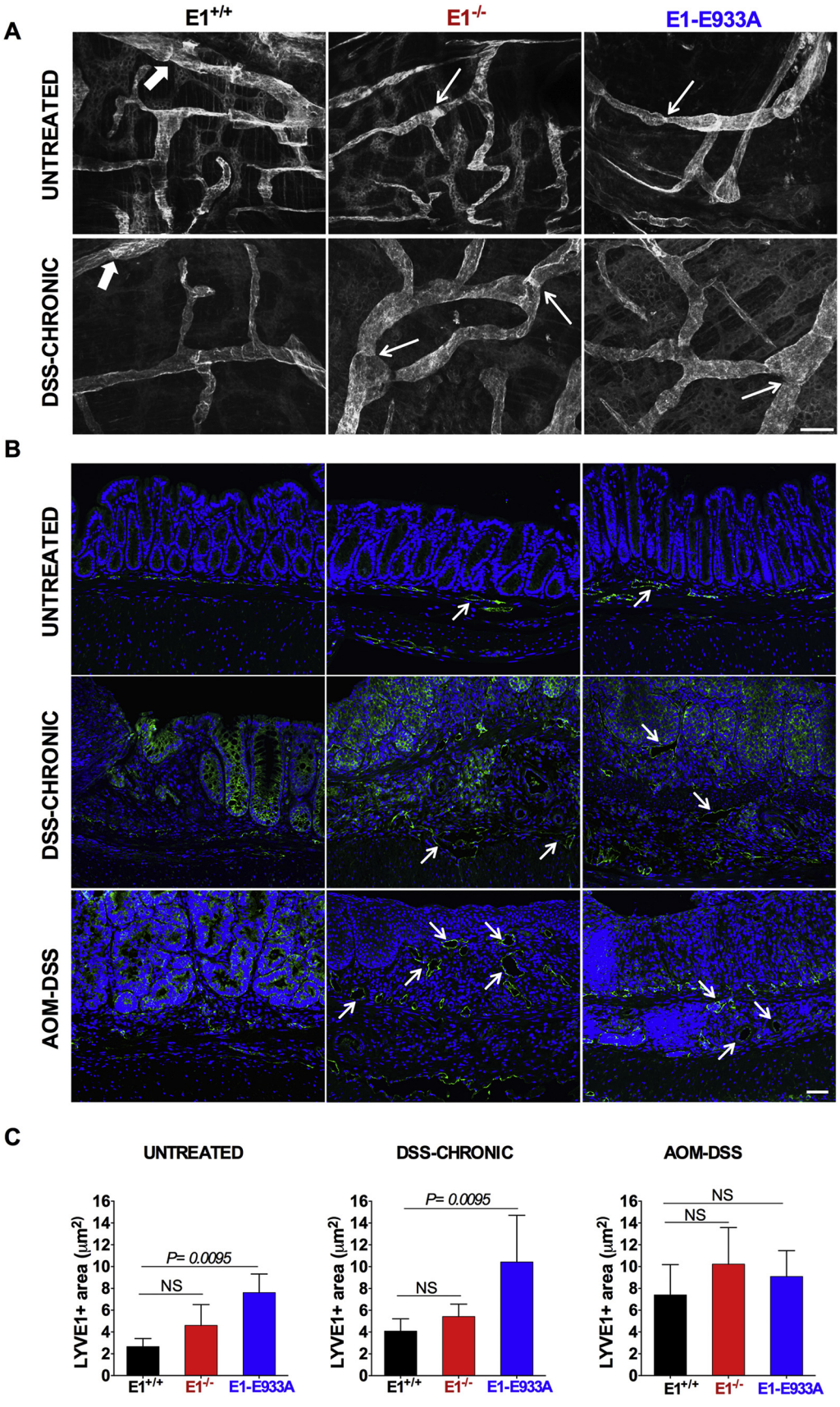
A
E1+/+
E1-/-
E1-E933A
UNTREATED
DSS-CHRONIC
B
UNTREATED
DSS-CHRONIC
AOM-DSS
C
UNTREATED
DSS-CHRONIC
AOM-DSS
LYVE1+ area (μm2)
P= 0.0095
NS
E1+/+
E1-/-
E1-E933A

DNA purification from agarose gels or for plasmid purification, as well as the restriction enzymes were purchased from Promega. T4 DNA Ligase was from New England Biolabs, and oligonucleotides were from Sigma Genosys. Recombinant human VEGF-C protein was purchased by R&D System. Anti−phospho-p44/42 MAPK (ERK1/2; Thr202/Tyr204), anti−phospho-AKT (Ser 473), anti-AKT and anti-ERK antibodies were obtained from Cell Signaling Technology. Goat anti-vinculin antibody was obtained from Santa Cruz Biotechnology, Inc. Anti VEGFR3 antibody was from R& D System, anti phospho-Tyr (clone 4G10) and anti GAPDH antibodies were purchased from Millipore.

Cells and cell procedures

Mouse LECs were isolated and immortalized according to the described procedure [18]. Briefly, mice were intraperitoneally injected with 200 μl of emulsified (1:1 with PBS) incomplete Freund's adjuvant (Sigma) twice, with a 15-day interval. Hyperplastic vessels were isolated from the liver and diaphragm at day 30 and treated with 0.5 mg/ml collagenase A (Roche Diagnostics), and the resulting single-cell suspension was cultured. After 7 to 10 days of culture, subconfluent cells were recovered with trypsin/EDTA, immortalized by means of SV40 infection. Immortalized LECs were characterized for lymphatic endothelial markers as we have previously reported [5]. Human LECs (HDLEC, Human Dermal Lymphatic Endothelial Cells, juvenile foreskin), and the media optimized for their growth were purchased from PromoCell GmbH.

Animals

C57Bl/6J and FVB mice were purchased from Charles River Laboratories. *Emilin1* $^{-/-}$ (E1 $^{-/-}$) and E1-E933A transgenic mice (C57Bl/6J and FVB backgrounds) were generated and maintained at the CRO-IRCCS mouse facility [20]. All animal procedures and their care were performed according to the institutional guidelines in compliance with national laws and with the authorization by the Italian Ministry of Health to Dr. Spessotto (n. 248/2015) and to Dr. Mongiat (n. 148/2016). Both for AOM/DSS colon carcinogenesis treatments and DSS-induced chronic/acute experimental colitis, we used 6/8 weeks aged female mice of each genotype (E1 $^{+/+}$, E1 $^{-/-}$ and E1-E933A).

Two-steps colon carcinogenesis (AOM/DSS)

C57BL/6 mice were treated with a single intraperitoneal injection of Azoxymethane (AOM, 7.4 mg/kg body weight, Sigma-Aldrich) followed by 1-week exposures (for a total of three times) to 2% dextran sulfate sodium salt (DSS, MP Biomedicals) in the drinking water (schedule in Fig. 1). Inflammation and tumor growth were observed over time by endoscopy (Karl Storz Veterinary Endoscopy), and at the end of the observation period (day 63) mice were sacrificed; clinical and endoscopic scoring of colitis were performed applying the Disease Activity Index (DAI) and the Murine Endoscopy Index of Colitis Severity (MEICS), respectively [59] (Supplemental Tables S1 and S2). Colon tissue samples were collected (recovering the part that goes from the cecum to the anus), measured and cut longitudinally. Differences in tumor number and volume between groups were first evaluated with gross anatomy examination of opened colons during necropsy; then colonic tissues were fixed, paraffin embedded and analyzed by immunohistochemistry or immunofluorescence. Colonic mucosa proliferative lesions (gastrointestinal intraepithelial neoplasia, low and high grade adenomas) were diagnosed according to the criteria described by Boivin et al. [60].

DSS-induced experimental colitis

Chronic colitis was induced with three 1-week exposures to 2% or 3% DSS (for C57BL/6 or FVB animals, respectively) in the drinking water (schedules in Figs. 3 and 4); the impact of intestinal inflammation was evaluated over time with DAI and MEICS scores. Mice were, then, sacrificed at day 63 (C57BL/6) or day 84 (FVB) and colon tissue samples were collected and treated as described in the above paragraph.

Blood samples collection

At the end of each treatment (colitis/colon carcinogenesis) a blood sample was collected by intracardiac sampling. Blood was recovered with 27 G (Becton, Dickinson and Co.), transferred in special tubes BD

Fig. 7. E1 $^{-/-}$ and E1-E933A transgenic mice display abnormal LV morphology and enhanced LV density in colon. (A) Representative images from whole mount colon samples stained with podoplanin from treated (chronic colitis) or untreated C57BL/6J animals. Thin and thick white arrows indicate abnormal (narrowed and ring-shaped) and normal (V-shaped) LV valves, respectively. (B) Representative images of IF staining of paraffin embedded colon sections with an antibody recognizing LYVE-1 performed on untreated, DSS-treated (chronic colitis) and AOM/DSS treated tissues. White arrows indicate enlarged LVs. Scale bar 50 μm. (C) Quantitative analysis of LV density; data are expressed as mean LYVE-1 positive area ± SD; statistical analysis was performed applying Mann Whitney U test; n = 5 animals per genotype for each treatment group; at least 8 fields per colon were considered.

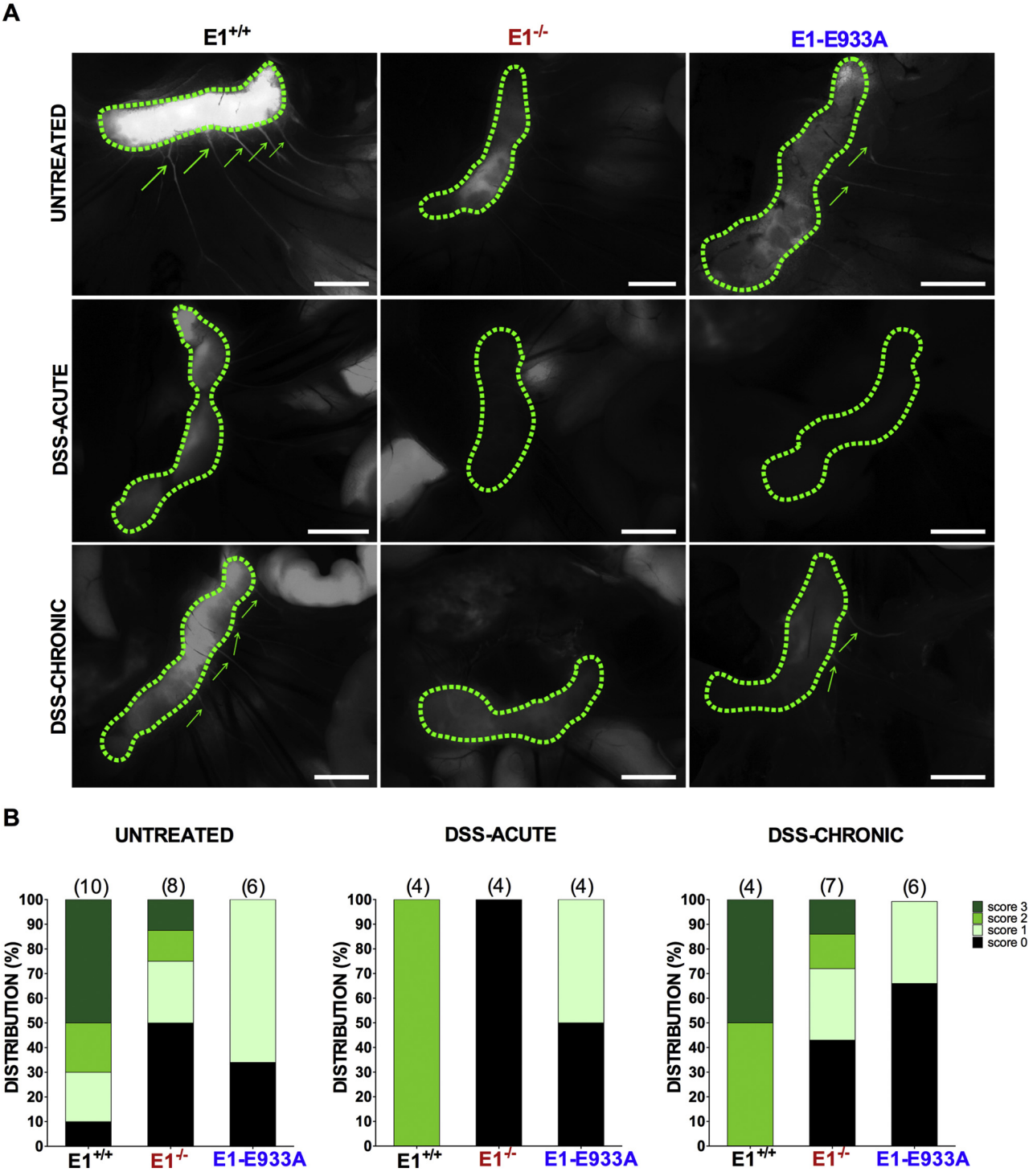

Fig. 8. E933A mutation in EMILIN-1 impairs mesenteric LV function. C57BL/6J mice with the different genotypes (treated or not for acute and chronic colitis) were submitted to mesenteric lymphangiography 2 h after oral administration of the fatty acid fluorescent dye Bodipy-FL-C_{16}. Mice were sacrificed and draining mesenteric lymph nodes (LNs) and mesenteric LVs were imaged with a fluorescence stereomicroscope. (A) Representative images are provided; scale bar: 2 mm. (B) Lymphangiography score distribution related to the three genotypes for each treatment group (the number of mice analyzed is indicated in parentheses). Mesenteric lymphangiographies were evaluated according to the following descriptive arbitrary score system: *score 0* = total absence of fluorescence in LNs and LV network; *score 1* = weak fluorescence in LNs and no LV network; *score 2* = weak/middle-intense fluorescent LNs and visible LV network; *score 3* = intense florescence in LNs and well-organized LV network.

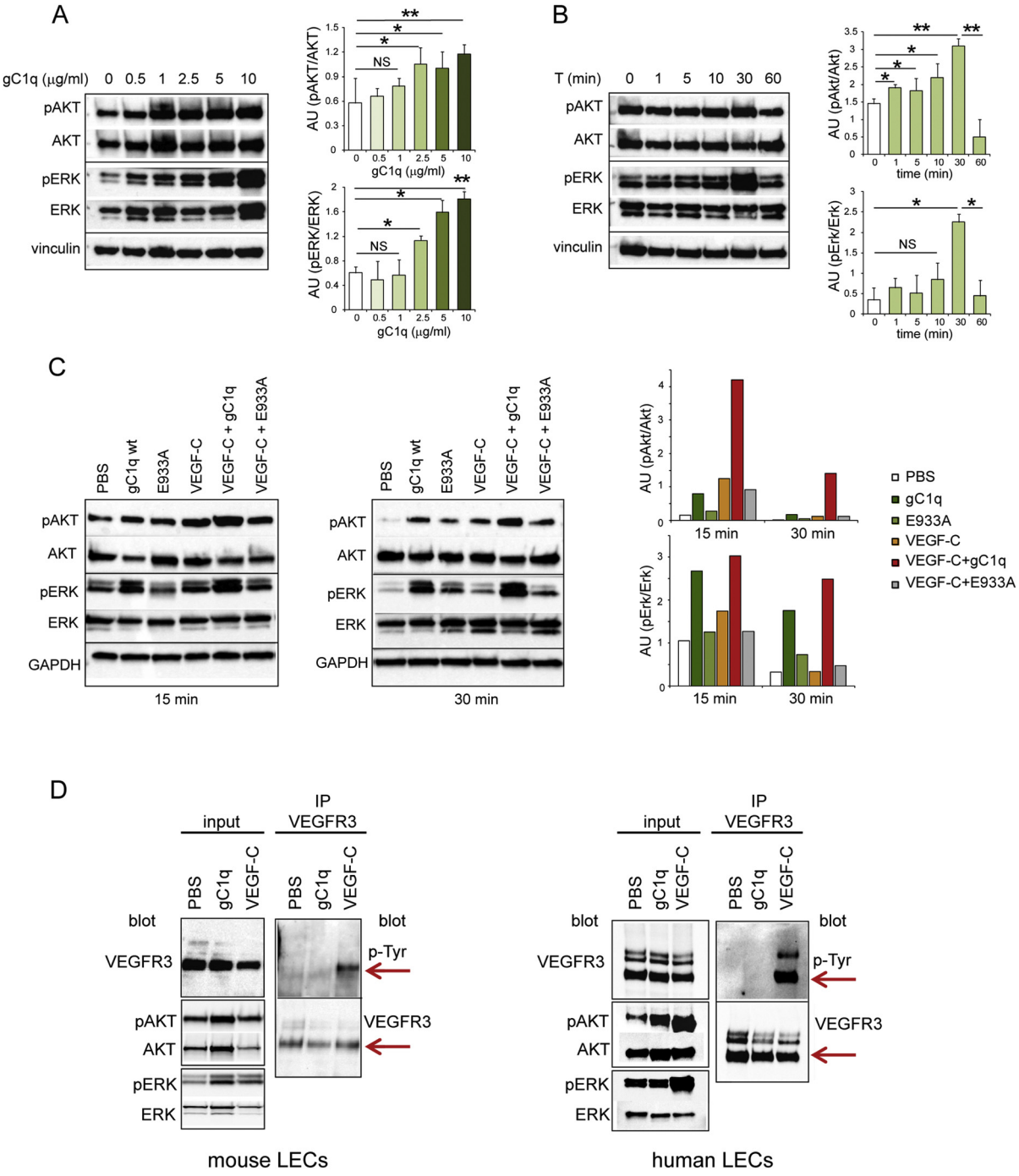

Fig. 9. EMILIN-1/β1 interaction associates with the activation of the lymphangiogenic pathway in LECs. Dose-response (A) and time-course (B) analysis of gC1q effect on AKT and ERK activation in LECs. Representative western blotting and the corresponding quantification of the ratio between the phosphorylated level and the total amount of the protein are displayed. Vinculin was used as loading normalization control. In the graphs the mean ± SD of 3 independent experiments is reported. *$P < 0.05$; **$P < 0.01$; NS, not significant. (C) Western blotting analyses of AKT and ERK pathway in LECs after stimulation for 15 (left) and 30 (middle) min with gC1q, gC1q mutant (E933A), VEGF-C and the combination of VEGF-C with gC1q or E933A. GAPDH was used as loading normalization control. The quantification of the corresponding signal ratio (pAKT/AKT and pERK/ERK) is reported on the graphs (right). (D) Immunoprecipitation (IP) of mouse (left) and human (right) LEC lysates after stimulation for 15 min with gC1q, VEGF-C, or PBS (negative control). Immunoprecipitates with VEGFR3 receptor were revealed with anti VEGFR3 and anti phospho-Tyr specific antibodies as indicated. Red arrows indicate VEGFR3 specific bands. The lysate corresponding activation levels of AKT and ERK are displayed.

Microtrainer® MAP K2EDTA 1.0 mg (Becton, Dickinson and Co.) to avoid blood coagulation and then analyzed to obtain the leucocyte formula using the Complete Blood Count (CBC) program.

Western blot and immunoprecipitation studies

Colonic samples were collected from AOM-DSS treated and untreated E1+/+, E1−/− and E1−/−/E1-E933A mice. Tissue extracts were prepared using the tissue protein extraction reagent lysis buffer (RIPA) supplemented with protease inhibitor cocktail (Roche, Basilea, Switzerland) following incubation on ice for 30 min. Cell extracts were obtained using a lysis buffer containing 50 mM Hepes pH 7.0, 250 mM NaCl, 5 mM EDTA, 0.5% NP40, 1 mM Na3VO4, 50 mM NaF and supplemented with protease inhibitor cocktail, following incubation on ice for 30 min. Samples were subjected to 4−20% SDS Page electrophoresis (using Criterion Precast Gel, BioRad) and blotted onto nitrocellulose membranes (Amersham Hybond-ECL, Amersham Pharmacia Biotech). Membranes were blocked (5% not fat milk, 0.1% Tween-20 in TBS) and incubated with specific and anti-vinculin (as loading control) primary antibodies. HRP-tagged secondary (GE Healthcare) antibodies were used. Signals were detected using Western Lightning ECL (Perkin Elmer). Membranes were analyzed on Biorad Chemidoc Touch Imaging System and quantified by Biorad ImageLab software.

Immunoprecipitates were performed as follows. LECs cells were starved in DMEM without serum for 24 h and then stimulated for 15 min at 37 °C with 10 μg/ml gC1q, 250 ng/ml VEGF-C or both (PBS was used as control). After washing with ice-cold PBS containing 0.1 mM Na3VO4, cells were solubilized with lysis buffer (Hepes 50 mM pH 7.0, 150 mM NaCl, 10% glycerol, 15 mM CHAPS, 1 mM Na3VO4, 25 mM NaF and supplemented with protease inhibitor cocktail), collected, and incubated on ice for 30 min. Cell lysates were centrifuged at 10,000*g* for 20 min, and quantified by Bradford assay (BioRad). 600−1000 μg of lysates were immunoprecipitated with anti VEGFR3 specific antibody ON at 4 °C and then incubated with 30 μl of Protein G Sepharose 4 Fast Flow resin (AmershamPharmacia Biotech) for 2 h at 4 °C. After incubation the solution was centrifuged at 6000*g* for 1 min and washed five times with HNTG buffer and at the end resuspended in 3× loading buffer. Immunoprecipitates were separated by 4−20% SDS Page electrophoresis, transferred to nitrocellulose, and immunoblotted with the specific anti phospho-tyrosine (clone 4G10) antibody.

Histopathology, immunohistochemistry and immunofluorescence analyses

After necropsy, 1 cm of the distal colon was recovered, fixed in 10% neutral buffered formalin for 48 h, transferred in 70% ethanol and then processed for paraffin embedding. For histopathological examination 4 or 5 μm-thick sections were obtained at the microtome, stained with hematoxylin and eosin (H&E) and examined with a light microscope for the detection and quantification of histological lesions; epithelial damage, inflammatory infiltrate and proliferative lesions were evaluated. For IHC analysis, serial sections were immunostained with the following primary antibodies: CD45/B220 (BD Pharmingen), CD3 epsilon (Santa Cruz), Ly6G (BD Biosciences), MPO (Dako) and Iba1 (Wako); sections were, then, incubated with biotinylated secondary (rabbit anti-rat or rabbit anti goat or goat anti-rabbit) antibodies and labeled by avidin-biotin-peroxidase system, using a commercial immunoperoxidase kit (Santa Cruz Biotechnology). Immunoreaction was visualized with 3,3′-diaminobenzidine (DAB) substrate and sections counterstained with Mayer's hematoxylin. All evaluation procedures were made in blind fashion. Positive signals were scored as described in figure legends. Counts were made at 400× and areas were chosen on the basis of more positive areas (hot spots areas). For IF analysis of LV density in colon tissues an anti Lyve-1 antibody (Abcam) was employed (overnight incubation at 4 °C) with the appropriate secondary antibody (Alexa Fluor® 488 conjugated anti rabbit, Life Technologies). For all samples, negative controls included corresponding isotype or IgG. To-Pro-3 (Life Technologies) was used to visualize nuclei. Images were acquired with a true confocal scanner system (TCS SP8 FSU AOBS, Leica Microsystems), equipped with a Leica DMi8 inverted microscope (Leica Microsystems). From 6 to 8 fields (20× magnification) were acquired and quantification (area) of the fluorescence positive structures was evaluated by means of the Volocity software (PerkinElmer Inc., Waltham, MA, USA).

Colons were also examined after whole mount staining approach. Untreated and treated colons were isolated, dissected and fixed in 4% PFA for 2 h at room temperature. After hydration for at least 48 h and permeabilization with PBS, 0.5% Triton X-100 buffer for 2 h, samples were incubated for 2 h with the blocking solution (PBS, BSA 1.5%). Later, an overnight incubation at 4 °C with an anti podoplanin monoclonal antibody (Abcam) was performed. After 5 washes with PBS 0.3% Triton X-100, the secondary anti hamster Alexa Fluor® 488 conjugated antibody was added for a 3 h incubation at room temperature. Samples were washed and mounted with Mowiol-2,5% DABCO; images were acquired with a confocal microscope (TCS SP8 FSU AOBS, Leica Microsystems), using Leica confocal LAS AF SP8 software.

In situ mesenteric lymphangiography

To visualize mesenteric LVs and to evaluate lymph node draining capacity, 1 ml of long-chain fatty acid,

Bodipy-FL-C_{16} (Life Technologies) was orally administered to $E1^{+/+}$, $E1^{-/-}$ and $E1^{-/-}$/E1-E933A C57Bl/6J DSS-treated and untreated mice. After 2 h from oral administration, mice were euthanized, and fluorescence imaging was performed in order to visualize labeled LVs and LNs in the mesentery, using a Leica M205 FA stereomicroscope (excitation light at 493 nm and emission light at 503 nm) equipped with a Leica DFC310 digital camera (Leica Microsystems).

Statistical analysis and data elaboration

Statistical significance of the results was determined by using the Mann Whitney *U* test to determine whether two datasets were significantly different. A value of $P < 0.05$ was considered significant.

Funding

This work was supported by the Ministry of Health, Italy [grant RF-2016-02361525 to Renato Cannizzaro and Paola Spessotto] and Associazione Italiana per la Ricerca sul Cancro (AIRC) [grant IG_14192 to PS].

Appendix A. Supplementary data

Supplementary data to this article can be found online at https://doi.org/10.1016/j.matbio.2019.08.006.

Received 20 May 2019;
Received in revised form 30 August 2019;
Accepted 30 August 2019
Available online 31 August 2019

Keywords:
Extracellular matrix;
Colitis-associated cancer;
Lymphatic aberrations

Abbreviations used:
DSS, dextran sulfate sodium; AOM, Azoxymethane; CAC, colitis associated cancer; ECM, extracellular matrix; LV, lymphatic vessel; LEC, lymphatic endothelial cell.

1 Present address, IOR – Institute of Oncology Research, Bellinzona, Switzerland.

2 These authors share co-last authorship.

References

[1] P. Spessotto, M. Cervi, M.T. Mucignat, G. Mungiguerra, I. Sartoretto, R. Doliana, A. Colombatti, Beta 1 integrin-dependent cell adhesion to EMILIN-1 is mediated by the gC1q domain, J. Biol. Chem. 278 (2003) 6160–6167. doi: https://doi.org/10.1074/jbc.M208322200.

[2] C. Danussi, A. Petrucco, B. Wassermann, E. Pivetta, T.M. Modica, L. Del Bel Belluz, A. Colombatti, P. Spessotto, EMILIN1-α4/α9 integrin interaction inhibits dermal fibroblast and keratinocyte proliferation, JCell Biol. 195 (2011) 131–145, https://doi.org/10.1083/jcb.201008013.

[3] C. Danussi, L. Del Bel Belluz, E. Pivetta, T.M. Modica, A. Muro, B. Wassermann, R. Doliana, P. Sabatelli, A. Colombatti, P. Spessotto, EMILIN1/alpha9beta1 integrin interaction is crucial in lymphatic valve formation and maintenance, MolCell Biol. 33 (2013) 4381–4394, https://doi.org/10.1128/MCB.00872-13.

[4] P. Spessotto, R. Bulla, C. Danussi, O. Radillo, M. Cervi, G. Monami, F. Bossi, F. Tedesco, R. Doliana, A. Colombatti, EMILIN1 represents a major stromal element determining human trophoblast invasion of the uterine wall, JCell Sci. 119 (2006) 4574–4584, https://doi.org/10.1242/jcs.03232.

[5] C. Danussi, A. Petrucco, B. Wassermann, T.M. Modica, E. Pivetta, L. Del Bel Belluz, A. Colombatti, P. Spessotto, An EMILIN1-negative microenvironment promotes tumor cell proliferation and lymph node invasion, Cancer PrevResPhila. 5 (2012) 1131–1143, https://doi.org/10.1158/1940-6207.CAPR-12-0076-T.

[6] S. Shawki, J. Ashburn, S.A. Signs, E. Huang, Colon cancer: inflammation-associated cancer, Surg. Oncol. Clin. N. Am. 27 (2018) 269–287, https://doi.org/10.1016/j.soc.2017.11.003.

[7] P.L. Lakatos, J. Burisch, Environment and invironment in IBDs: partners in crime, Gut. 64 (2015) 1009–1010, https://doi.org/10.1136/gutjnl-2014-308460.

[8] R.A. Risques, L.A. Lai, C. Himmetoglu, A. Ebaee, L. Li, Z. Feng, M.P. Bronner, B. Al-Lahham, K.V. Kowdley, K.D. Lindor, P.S. Rabinovitch, T.A. Brentnall, Ulcerative colitis-associated colorectal cancer arises in a field of short telomeres, senescence, and inflammation, Cancer Res. 71 (2011) 1669–1679, https://doi.org/10.1158/0008-5472.CAN-10-1966.

[9] L. Vermeulen, E. Morrissey, M. van der Heijden, A.M. Nicholson, A. Sottoriva, S. Buczacki, R. Kemp, S. Tavare, D.J. Winton, Defining stem cell dynamics in models of intestinal tumor initiation, Science. 342 (2013) 995–998, https://doi.org/10.1126/science.1243148.

[10] S.I. Grivennikov, F.R. Greten, M. Karin, Immunity, inflammation, and cancer, Cell. 140 (2010) 883–899, https://doi.org/10.1016/j.cell.2010.01.025.

[11] R. Francescone, V. Hou, S.I. Grivennikov, Cytokines, IBD, and colitis-associated cancer, Inflamm. Bowel Dis. 21 (2015) 409–418, https://doi.org/10.1097/MIB.0000000000000236.

[12] E. Brauchle, J. Kasper, R. Daum, N. Schierbaum, C. Falch, A. Kirschniak, T.E. Schäffer, K. Schenke-Layland, Biomechanical and biomolecular characterization of extracellular matrix structures in human colon carcinomas, Matrix Biol. J. Int. Soc. Matrix Biol. 68–69 (2018) 180–193, https://doi.org/10.1016/j.matbio.2018.03.016.

[13] A.C. Petrey, C.A. de la Motte, Hyaluronan in inflammatory bowel disease: cross-linking inflammation and coagulation, Matrix Biol. 78–79 (2018) 314–323, https://doi.org/10.1016/j.matbio.2018.03.011.

[14] K. Alitalo, T. Tammela, T.V. Petrova, Lymphangiogenesis in development and human disease, Nature. 438 (2005) 946–953, https://doi.org/10.1038/nature04480.

[15] H. Kim, R.P. Kataru, G.Y. Koh, Inflammation-associated lymphangiogenesis: a double-edged sword? J. Clin. Invest. 124 (2014) 936–942, https://doi.org/10.1172/JCI71607.

[16] S. Vetrano, E.M. Borroni, A. Sarukhan, B. Savino, R. Bonecchi, C. Correale, V. Arena, M. Fantini, M. Roncalli,

A. Malesci, A. Mantovani, M. Locati, S. Danese, The lymphatic system controls intestinal inflammation and inflammation-associated colon cancer through the chemokine decoy receptor D6, Gut. 59 (2010) 197–206, https://doi.org/10.1136/gut.2009.183772.
[17] N.B. Piller, Macrophage and tissue changes in the developmental phases of secondary lymphoedema and during conservative therapy with benzopyrone, Arch. Histol. Cytol. 53 (Suppl) (1990) 209–218.
[18] C. Danussi, P. Spessotto, A. Petrucco, B. Wassermann, P. Sabatelli, M. Montesi, R. Doliana, G.M. Bressan, A. Colombatti, Emilin1 deficiency causes structural and functional defects of lymphatic vasculature, MolCell Biol. 28 (2008) 4026–4039, https://doi.org/10.1128/MCB.02062-07.
[19] E. Pivetta, B. Wassermann, L. Del Bel Belluz, C. Danussi, T.M. Modica, O. Maiorani, G. Bosisio, F. Boccardo, V. Canzonieri, A. Colombatti, P. Spessotto, Local inhibition of elastase reduces EMILIN1 cleavage reactivating lymphatic vessel function in a mouse lymphoedema model, Clin. Sci.(Lond) 130 (2016) 1221–1236, https://doi.org/10.1042/CS20160064.
[20] A. Capuano, F. Fogolari, F. Bucciotti, P. Spessotto, P.A. Nicolosi, M.T. Mucignat, M. Cervi, G. Esposito, A. Colombatti, R. Doliana, The α4β1/EMILIN1 interaction discloses a novel and unique integrin-ligand type of engagement, Matrix Biol. J. Int. Soc. Matrix Biol. 66 (2018) 50–66, https://doi.org/10.1016/j.matbio.2017.10.001.
[21] A. Capuano, E. Pivetta, F. Baldissera, G. Bosisio, B. Wassermann, F. Bucciotti, A. Colombatti, P. Sabatelli, R. Doliana, P. Spessotto, Integrin binding site within the gC1q domain orchestrates EMILIN-1-induced lymphangiogenesis, Matrix Biol. J. Int. Soc. Matrix Biol. 81 (2019) 34–49, https://doi.org/10.1016/j.matbio.2018.10.006.
[22] T. Tanaka, H. Kohno, R. Suzuki, Y. Yamada, S. Sugie, H. Mori, A novel inflammation-related mouse colon carcinogenesis model induced by azoxymethane and dextran sodium sulfate, Cancer Sci. 94 (2003) 965–973.
[23] S. Wirtz, M.F. Neurath, Mouse models of inflammatory bowel disease, Adv. Drug Deliv. Rev. 59 (2007) 1073–1083, https://doi.org/10.1016/j.addr.2007.07.003.
[24] K. Fu, Y. Tsujinaka, Y. Hamahata, K. Matsuo, O. Tsutsumi, Squamous metaplasia of the rectum associated with ulcerative colitis diagnosed using narrow-band imaging, Endoscopy. 40 (Suppl. 2) (2008) E45–E46, https://doi.org/10.1055/s-2007-966861.
[25] S. D'Alessio, C. Correale, C. Tacconi, A. Gandelli, G. Pietrogrande, S. Vetrano, M. Genua, V. Arena, A. Spinelli, L. Peyrin-Biroulet, C. Fiocchi, S. Danese, VEGF-C-dependent stimulation of lymphatic function ameliorates experimental inflammatory bowel disease, J. Clin. Invest. 124 (2014) 3863–3878, https://doi.org/10.1172/JCI72189.
[26] G.R. Abouelkheir, B.D. Upchurch, J.M. Rutkowski, Lymphangiogenesis: fuel, smoke, or extinguisher of inflammation's fire? Exp. Biol. Med. Maywood NJ. 242 (2017) 884–895, https://doi.org/10.1177/1535370217697385.
[27] F. Zhou, Z. Chang, L. Zhang, Y.-K. Hong, B. Shen, B. Wang, F. Zhang, G. Lu, D. Tvorogov, K. Alitalo, B.A. Hemmings, Z. Yang, Y. He, Akt/protein kinase B is required for lymphatic network formation, remodeling, and valve development, Am. J. Pathol. 177 (2010) 2124–2133, https://doi.org/10.2353/ajpath.2010.091301.
[28] Y. Deng, D. Atri, A. Eichmann, M. Simons, Endothelial ERK signaling controls lymphatic fate specification, J. Clin. Invest. 123 (2013) 1202–1215, https://doi.org/10.1172/JCI63034.
[29] K. Rauniyar, S.K. Jha, M. Jeltsch, Biology of vascular endothelial growth factor C in the morphogenesis of lymphatic vessels, Front. Bioeng. Biotechnol. 6 (2018) 7, https://doi.org/10.3389/fbioe.2018.00007.
[30] T. Mäkinen, T. Veikkola, S. Mustjoki, T. Karpanen, B. Catimel, E.C. Nice, L. Wise, A. Mercer, H. Kowalski, D. Kerjaschki, S.A. Stacker, M.G. Achen, K. Alitalo, Isolated lymphatic endothelial cells transduce growth, survival and migratory signals via the VEGF-C/D receptor VEGFR-3, EMBO J. 20 (2001) 4762–4773, https://doi.org/10.1093/emboj/20.17.4762.
[31] N. Nagy, H.F. Kuipers, P.L. Marshall, E. Wang, G. Kaber, P.L. Bollyky, Hyaluronan in immune dysregulation and autoimmune diseases, Matrix Biol. 78–79 (2019) 292–313, https://doi.org/10.1016/j.matbio.2018.03.022.
[32] B.-H. Gu, M.C. Madison, D. Corry, F. Kheradmand, Matrix remodeling in chronic lung diseases, Matrix Biol. J. Int. Soc. Matrix Biol. 73 (2018) 52–63, https://doi.org/10.1016/j.matbio.2018.03.012.
[33] J.H. Mortensen, T. Manon-Jensen, M.D. Jensen, P. Hägglund, L.G. Klinge, J. Kjeldsen, A. Krag, M.A. Karsdal, A.-C. Bay-Jensen, Ulcerative colitis, Crohn's disease, and irritable bowel syndrome have different profiles of extracellular matrix turnover, which also reflects disease activity in Crohn's disease, PLoS One 12 (2017), e0185855, https://doi.org/10.1371/journal.pone.0185855.
[34] C. Zeltz, D. Gullberg, Post-translational modifications of integrin ligands as pathogenic mechanisms in disease, Matrix Biol. J. Int. Soc. Matrix Biol. 40 (2014) 5–9, https://doi.org/10.1016/j.matbio.2014.08.001.
[35] K. Rilla, A.-M. Mustonen, U.T. Arasu, K. Härkönen, J. Matilainen, P. Nieminen, Extracellular vesicles are integral and functional components of the extracellular matrix, Matrix Biol. J. Int. Soc. Matrix Biol. 75–76 (2019) 201–219, https://doi.org/10.1016/j.matbio.2017.10.003.
[36] E.W. Law, A.K. Cheung, V.I. Kashuba, T.V. Pavlova, E.R. Zabarovsky, H.L. Lung, Y. Cheng, D. Chua, K.D. Lai-Wan, S.W. Tsao, T. Sasaki, E.J. Stanbridge, M.L. Lung, Anti-angiogenic and tumor-suppressive roles of candidate tumor-suppressor gene, Fibulin-2, in nasopharyngeal carcinoma, Oncogene. 31 (2012) 728–738, https://doi.org/10.1038/onc.2011.272.
[37] S. Marastoni, E. Andreuzzi, A. Paulitti, R. Colladel, R. Pellicani, F. Todaro, A. Schiavinato, P. Bonaldo, A. Colombatti, M. Mongiat, EMILIN2 down-modulates the Wnt signalling pathway and suppresses breast cancer cell growth and migration, J. Pathol. 232 (2014) 391–404, https://doi.org/10.1002/path.4316.
[38] T. Neill, L. Schaefer, R.V. Iozzo, Oncosuppressive functions of decorin, Mol. Cell. Oncol. 2 (2015), e975645, https://doi.org/10.4161/23723556.2014.975645.
[39] R. Hirani, E. Hanssen, M.A. Gibson, LTBP-2 specifically interacts with the amino-terminal region of fibrillin-1 and competes with LTBP-1 for binding to this microfibrillar protein, Matrix Biol. 26 (2007) 213–223, https://doi.org/10.1016/j.matbio.2006.12.006.
[40] M.K. Parsi, J.R. Adams, J. Whitelock, M.A. Gibson, LTBP-2 has multiple heparin/heparan sulfate binding sites, Matrix Biol. 29 (2010) 393–401, https://doi.org/10.1016/j.matbio.2010.03.005.
[41] K. Wang, F. Wu, B.R. Seo, C. Fischbach, W. Chen, L. Hsu, D. Gourdon, Breast cancer cells alter the dynamics of stromal fibronectin-collagen interactions, Matrix Biol. J. Int. Soc. Matrix Biol. 60–61 (2017) 86–95, https://doi.org/10.1016/j.matbio.2016.08.001.

[42] L.A. Griggs, N.T. Hassan, R.S. Malik, B.P. Griffin, B.A. Martinez, L.W. Elmore, C.A. Lemmon, Fibronectin fibrils regulate TGF-β1-induced epithelial-mesenchymal transition, Matrix Biol. J. Int. Soc. Matrix Biol. 60–61 (2017) 157–175, https://doi.org/10.1016/j.matbio.2017.01.001.

[43] A.Y. Liu, H. Zheng, G. Ouyang, Periostin, a multifunctional matricellular protein in inflammatory and tumor microenvironments, Matrix Biol. J. Int. Soc. Matrix Biol. 37 (2014) 150–156, https://doi.org/10.1016/j.matbio.2014.04.007.

[44] P. Moreno-Layseca, C.H. Streuli, Signalling pathways linking integrins with cell cycle progression, Matrix Biol. 34 (2014) 144–153, https://doi.org/10.1016/j.matbio.2013.10.011.

[45] S.S. Skandalis, N. Afratis, G. Smirlaki, D. Nikitovic, A.D. Theocharis, G.N. Tzanakakis, N.K. Karamanos, Cross-talk between estradiol receptor and EGFR/IGF-IR signaling pathways in estrogen-responsive breast cancers: focus on the role and impact of proteoglycans, Matrix Biol. J. Int. Soc. Matrix Biol. 35 (2014) 182–193, https://doi.org/10.1016/j.matbio.2013.09.002.

[46] D. Nikitovic, A. Papoutsidakis, N.K. Karamanos, G.N. Tzanakakis, Lumican affects tumor cell functions, tumor-ECM interactions, angiogenesis and inflammatory response, Matrix Biol. J. Int. Soc. Matrix Biol. 35 (2014) 206–214, https://doi.org/10.1016/j.matbio.2013.09.003.

[47] L. Zacchigna, C. Vecchione, A. Notte, M. Cordenonsi, S. Dupont, S. Maretto, G. Cifelli, A. Ferrari, A. Maffei, C. Fabbro, P. Braghetta, G. Marino, G. Selvetella, A. Aretini, C. Colonnese, U. Bettarini, G. Russo, S. Soligo, M. Adorno, P. Bonaldo, D. Volpin, S. Piccolo, G. Lembo, G.M. Bressan, Emilin1 links TGF-beta maturation to blood pressure homeostasis, Cell. 124 (2006) 929–942, https://doi.org/10.1016/j.cell.2005.12.035.

[48] A.H. Györfi, A.-E. Matei, J.H.W. Distler, Targeting TGF-β signaling for the treatment of fibrosis, Matrix Biol. J. Int. Soc. Matrix Biol. 68–69 (2018) 8–27, https://doi.org/10.1016/j.matbio.2017.12.016.

[49] T. Avraham, S. Daluvoy, J. Zampell, A. Yan, Y.S. Haviv, S.G. Rockson, B.J. Mehrara, Blockade of transforming growth factor-beta1 accelerates lymphatic regeneration during wound repair, Am. J. Pathol. 177 (2010) 3202–3214, https://doi.org/10.2353/ajpath.2010.100594.

[50] M.F. Neurath, Cytokines in inflammatory bowel disease, Nat. Rev. Immunol. 14 (2014) 329–342, https://doi.org/10.1038/nri3661.

[51] S. Danese, A. Mantovani, Inflammatory bowel disease and intestinal cancer: a paradigm of the Yin-Yang interplay between inflammation and cancer, Oncogene. 29 (2010) 3313–3323, https://doi.org/10.1038/onc.2010.109.

[52] J.F. Wang, X.F. Zhang, J.E. Groopman, Stimulation of beta 1 integrin induces tyrosine phosphorylation of vascular endothelial growth factor receptor-3 and modulates cell migration, J. Biol. Chem. 276 (2001) 41950–41957, https://doi.org/10.1074/jbc.M101370200.

[53] X. Zhang, J.E. Groopman, J.F. Wang, Extracellular matrix regulates endothelial functions through interaction of VEGFR-3 and integrin alpha5beta1, J. Cell. Physiol. 202 (2005) 205–214, https://doi.org/10.1002/jcp.20106.

[54] J. Goldman, T.X. Le, M. Skobe, M.A. Swartz, Overexpression of VEGF-C causes transient lymphatic hyperplasia but not increased lymphangiogenesis in regenerating skin, Circ. Res. 96 (2005) 1193–1199, https://doi.org/10.1161/01.RES.0000168918.27576.78.

[55] O. Maiorani, E. Pivetta, A. Capuano, T.M. Modica, B. Wassermann, F. Bucciotti, A. Colombatti, R. Doliana, P. Spessotto, Neutrophil elastase cleavage of the gC1q domain impairs the EMILIN1-alpha4beta1 integrin interaction, cell adhesion and anti-proliferative activity, Sci. Rep. 7 (2017) 39974, https://doi.org/10.1038/srep39974.

[56] K. Shang, Y.-P. Bai, C. Wang, Z. Wang, H.-Y. Gu, X. Du, X.-Y. Zhou, C.-L. Zheng, Y.-Y. Chi, N. Mukaida, Y.-Y. Li, Crucial involvement of tumor-associated neutrophils in the regulation of chronic colitis-associated carcinogenesis in mice, PLoS One 7 (2012), e51848, https://doi.org/10.1371/journal.pone.0051848.

[57] Y. Morohoshi, K. Matsuoka, H. Chinen, N. Kamada, T. Sato, T. Hisamatsu, S. Okamoto, N. Inoue, H. Takaishi, H. Ogata, Y. Iwao, T. Hibi, Inhibition of neutrophil elastase prevents the development of murine dextran sulfate sodium-induced colitis, J. Gastroenterol. 41 (2006) 318–324, https://doi.org/10.1007/s00535-005-1768-8.

[58] R. Mizuno, K. Kawada, Y. Itatani, R. Ogawa, Y. Kiyasu, Y. Sakai, The role of tumor-associated neutrophils in colorectal cancer, Int. J. Mol. Sci. 20 (2019). doi:https://doi.org/10.3390/ijms20030529.

[59] C. Becker, M.C. Fantini, S. Wirtz, A. Nikolaev, R. Kiesslich, H.A. Lehr, P.R. Galle, M.F. Neurath, In vivo imaging of colitis and colon cancer development in mice using high resolution chromoendoscopy, Gut. 54 (2005) 950–954, https://doi.org/10.1136/gut.2004.061283.

[60] G.P. Boivin, K. Washington, K. Yang, J.M. Ward, T.P. Pretlow, R. Russell, D.G. Besselsen, V.L. Godfrey, T. Doetschman, W.F. Dove, H.C. Pitot, R.B. Halberg, S.H. Itzkowitz, J. Groden, R.J. Coffey, Pathology of mouse models of intestinal cancer: consensus report and recommendations, Gastroenterology. 124 (2003) 762–777, https://doi.org/10.1053/gast.2003.50094.